PCCP

Effects of Molecular Size and Orientation on Interfacial Properties and Wetting Behavior of Water/n-Alkane Systems: A Molecular-Dynamics Study

Journal:	*Physical Chemistry Chemical Physics*
Manuscript ID	CP-ART-12-2022-005735.R1
Article Type:	Paper
Date Submitted by the Author:	23-Jan-2023
Complete List of Authors:	Hrahsheh, Fawaz; Higher Colleges of Technology, ETS Wilemski, Gerald; Missouri University of Science and Technology, Department of Physics

Journal Name

ARTICLE TYPE

Cite this: DOI: 00.0000/xxxxxxxxxx

Effects of Molecular Size and Orientation on Interfacial Properties and Wetting Behavior of Water/n-Alkane Systems: A Molecular-Dynamics Study†

Fawaz Hrahsheh,[a] Gerald Wilemski,[b]

Received Date
Accepted Date

DOI: 00.0000/xxxxxxxxxx

Molecular dynamics simulations (MD) are performed to study the interfacial structure/tension and wetting behavior of water/n-alkane systems (water/nC5 to water/nC16 where nCx=CxH(2x+2)). In particular, we study complete-to-partial wetting transitions by changing n-alkane chain lengths (N_C) at constant temperature, $T = 295K$. Simulations are carried out with a united-atom TraPPE model for n-alkanes and the TIP4P-2005 model of water. Simulation results are in excellent agreement with initial spreading coefficients and contact angles calculated using experimental values of surface and interfacial tensions. Additionally, it has been determined that water/(nC5-nC7) and water/(nC8-nC16), respectively, exhibit complete and partial initial wetting modes. Simulations show that the interfacial structures of water/(nC5-nC7) are different from water/(nC8-nC16) systems. In the latter, water preferentially orients near the interface to increase the number of hydrogen bonds and the charge and mass densities. Moreover, the orientation of n-alkane molecules at water/(nC8-nC16) interfaces has a long-range persistence resulting in layered structures that increase with N_C. In addition, simulation results of the orientational order parameter S_z show alignment behavior of n-alkane molecules with respect to the interfaces. Simulations predict that the central segments of n-alkane are strongly packed in the interfaces while the end segments (methyl groups) form smaller peaks in the outer edge of the layer. This observation confirms the "horseshoe" or "C-shaped" structure of n-alkane molecules in the water/n-alkane interfaces. At constant temperature, the interface widths of both water and the n-alkanes decrease with increasing n-alkane molecular length. These results suggest that increasing the n-alkane chain length affects the water/n-alkane interfacial properties in a manner similar to that of cooling.

1 Introduction

Many investigations have been performed to study aqueous/organic interfaces because of their relevance in environmental and industrial applications. Alkanes are organic molecules that are extensively used to study such interfaces because of their simple chain structure. Moreover, they form the main building block of more complex organic compounds.[1–7] Similar to the mutual solubility of water/organic mixtures, wetting behavior is a key feature in the field of aqueous/organic interfaces. In general, the degree of wetting, i.e., partial or complete, will be determined by the balance of surface free energies of the materials involved. Surface free energy is the excess energy that the surface has compared to the bulk phase of the material. In the bulk, because of isotropy and symmetry, molecules experience a zero-net force on average. On the other hand, interfaces are inherently anisotropic and inhomogeneous, and this loss of symmetry results in the surface free energy. The magnitude of the surface free energy depends on the interaction between the molecules. In the case of water, the surface free energy is high due to strong hydrogen bonds and dipole-dipole interactions between the water molecules. In n-alkanes, the molecular forces are typically much weaker, and thus the surface free energy of the n-alkanes is low.

For decades, n-alkane systems (particularly pentane, hexane, and heptane) have been theoretically and experimentally studied to determine whether or not they spread over water under ambient conditions.[8–18] Because many of the results were contradictory, it had been difficult to reach a consensus on the equilibrium wetting behavior. Subsequent work has established a more consistent picture in which pentane and all longer n-alkanes do not wet water at room temperature.[14,17,19–22]

[a] Higher Colleges of Technology, ETS, MZWC, Abu Dhabi, 58855, UAE.
[b] Department of Physics, Missouri University of Science and Technology, Rolla, MO 65409, USA.
[a] E-mail: fhrahsheh@hct.ac.ae/fyh44f@umsystem.edu
[b] E-mail: wilemski@mst.edu

† Electronic Supplementary Information (ESI) available: Additional supporting material is provided. Additional data related to this paper may be requested from the authors. See DOI: 00.0000/00000000.

In this work, we study water/n-alkane interfacial properties, particularly the initial wetting behavior, using molecular-dynamics simulations. Because it is not easy to calculate the surface free energy, water/n-alkane wetting is usually determined by an equivalent property, the interfacial tension. For the complete wetting, the water-vapor surface tension (γ_{wv}) exceeds the sum of water-alkane (γ_{wa}) and alkane-vapor (γ_{av}) surface tensions, ($\gamma_{wv} > \gamma_{wa} + \gamma_{av}$), while for the partial wetting the water-vapor surface tension is smaller than them, ($\gamma_{wv} < \gamma_{wa} + \gamma_{av}$). According to Rowlinson and Widom,[23] these inequality formulas are actually equivalent to the so-called spreading coefficient,

$$S = \gamma_{wv} - (\gamma_{wa} + \gamma_{av}), \tag{1}$$

which must be negative to fulfill the condition for equilibrium of three phases at a line of mutual contact. Transitions between complete and partial wetting of oil on water can occur induced by variation of several parameters including, but not limited to, changing temperature,[24] tuning the mutual interactions,[25] and adding salt/surfactants.[5,26,27]

From molecular simulations, the average surface tension γ is readily calculated from the difference between normal and lateral values of pressure as follows:[28]

$$\gamma = \frac{L_z}{2}\left[\langle P_n\rangle - \langle P_t\rangle\right]. \tag{2}$$

Here, L_z is the length of the simulation box normal to the interface, $\langle P_n\rangle$ and $\langle P_t\rangle$ are the mean pressure tensors normal (z) and tangential (xy) to the interface. They are averaged over 150 ns of NVT simulations after 10 ns of equilibration.

To assess the reliability of our simulations, we compare our results for spreading coefficients and contact angles with calculations based on the experimental data of Goebel and Lunkenheimer.[1,29] These researchers made several purification cycles to determine the water/oil interfacial tensions using the ring method with accuracies reaching $\pm 0.2\%$ at 295 K. We also compare our results with measurements of Zeppieri et al.[2]

In this work, we use equilibrium molecular dynamic simulations to study water/n-alkane interfaces at constant temperature, $T = 295\ K$. Fixing the simulation temperature enables us to investigate the effects of n-alkane chain lengths N_C on the wetting behavior. Here, we denote n-alkanes symbolically as nCx such as nC5 for normal-pentane and nC16 for normal-hexadecane. In addition to the spreading coefficient S, we also calculate the water/nCx contact angles, θ_c, using a rigorously derived formula,[23]

$$\cos(\theta_c) = \frac{\gamma_{wv}^2 - \gamma_{wa}^2 - \gamma_{av}^2}{2\gamma_{wa}\gamma_{av}}. \tag{3}$$

To calculate the spreading coefficients and contact angles using equation (1) and equation (3), we determine the interfacial tensions of pure water/vapor, pure nCx/vapor, and water/nCx at $T = 295\ K$.*

We can monitor the n-alkane chain orientation in the interfaces using an orientational order parameter S_z defined in terms of the angle ϕ between the interface normal vector (the director) and some vector describing the local orientation of the molecule. The vector connecting a pair of carbon atoms that are two units apart in a molecule (e.g., atoms 1 and 3) is found to be a convenient vector for this parameter.[30,31] This order parameter is actually the second Legendre polynomial of $cos(\phi)$ averaged over all vectors and time steps. Thus, it is defined as:

$$S_z = \frac{3\left\langle cos^2(\phi)\right\rangle - 1}{2}. \tag{4}$$

The order parameter S_z provides a convenient quantification of alignment: $S_z = 1$ denotes perfect alignment (along the director), $0 < S_z < 1$ denotes partial alignment, $S_z = 0$ denotes a completely random alignment, and $S_z = -1/2$ denotes complete perpendicular-alignment to the director.

2 Methods and Simulation Settings

Two united-atom (UA) force fields are initially used to model n-alkanes: PYS (Paul, Yoon, Smith)[32–34] and TraPPE (Transferable Potentials for Phase Equilibria)[35–38]. These united-atom force fields have been widely used to study thermodynamic properties of alkanes including phase-equilibria, interfacial properties, and phase transitions.[24,39–47] Water is modeled with a rigid four-site model TIP4P-2005 which consists of three fixed point charges (two hydrogen atoms HW1 and HW2, and one virtual site M) and one Lennard-Jones center (neutral oxygen atom O).[48] The surface tension of the TIP4P-2005 model has been studied using several methods that confirm the validity and reliability of this model.[49–52] One of the main differences between the PYS and TraPPE models is that the PYS assumes both methyl and methylene groups interact identically with water.

Molecular dynamic simulations in this work are performed using the GROMACS software package.[53–56] The classical equations of motions are integrated with the velocity Verlet algorithm[57] with a time-step of 5 fs.† We use periodic simulation cells in the three directions and we control the temperature using the v-rescale thermostat[58] with time constant of 0.2 ps. A fast and stable algorithm (LINC algorithm) is used to maintain the water molecule rigidity.[59] The electrostatic interactions were implemented using a Particle-mesh Ewald method.[60] All the nC-nC, water-water, and water-nC interactions are cut-off at 1.5 nm. Although the long-range van der Waals tail corrections to the energy and pressure are accurate for homogeneous systems with a long cut-off, they don't directly treat the properties of inhomogeneous systems such as interfacial tensions.[61] For such cases, a variant of the Particle Mesh Ewald algorithm was already proposed for the Lennard-Jones dispersion interactions (LJ-PME),[62] but it was implemented only recently in GROMACS.[63] This method is used here, and it allows surface tensions of liquids as well as bulk prop-

* As discussed elsewhere[24], only initial spreading coefficients and contact angles are determined here, but for simplicity we omit repeating the word "initial".

† Using the LJ-PME enables us to use larger timestep (5 fs) with $r_c = 1.5\ nm$. Our results of surface tensions agree with the results of P. Neupane and G. Wilemski work (Supplementary Material),[24] where they implemented the LJ potential using the cut-off method with a long cut-off radius $r_c = 2.4\ nm$ and 1 fs timestep, and including the long-range tail correction.

erties, such as density, to be determined without approximations due to truncation.[61,64,65]

In this work, MD simulations of water/n-alkane systems are performed for one slab of water placed between two slabs of n-alkane. In addition to the temperature, we fix the number of molecules and the simulation box volume in NVT simulations. Therefore, increasing the n-alkane chain length decreases the vapor-to-liquid volume ratio. This occurrence leads to significant effects on the simulation conditions (and hence the system pressure, liquid-vapor equilibrium, and interfacial tensions). To keep the NVT conditions same for all water/n-alkane simulations, we fix the number of carbon atoms for all n-alkanes instead of the number of molecules. We begin with the longest n-alkane chain in our study (nC16) because it needs simulation slabs to be thick enough to avoid any correlation between its nC16/vapor and water/nC16 interfaces. We find that 2400 carbon atoms and 1500 water molecules in $3.5 \times 3.5 \times 25\ nm^3$ is sufficient to have isotropic bulk phases for all n-alkanes systems in our study (nC5-nC16). The vapor phase in the Z direction is thick enough so that the two n-alkane/vapor interfaces do not interact with each other even though periodic boundary conditions are imposed. The MD simulations of pure n-alkane and water are performed with the same number of molecules in the corresponding water/n-alkane systems and in simulation boxes three times larger than the liquid thickness, $5 \times 5 \times 15\ nm^3$.

3 Results and Discussion

To compare with the measurements of interfacial tensions of Goebel and Lunkenheimer[1] at $T = 295\ K$, we have calculated the interfacial tension of a set of n-alkane systems using two different models (PYS and TraPPE). As shown in Figure 1, the dependence of the PYS surface tension on N_C is very high compared to the experimental values.[1] Thus, using the PYS force field requires tuning separately the water/n-alkane interaction strength ε_{OC} for every n-alkane, which is very expensive computationally. This behavior of the surface tension for the PYS model needs more investigation, particularly regarding its effect on interfaces.

To avoid this complication, we have decided to use the TraPPE-UA force field in modeling our n-alkane systems. Surface tensions of n-alkanes using TraPPE-UA model agree fairly well with the experimental values (Figure 1) in magnitude and in the rate of change with N_C.[1]

To further confirm the reliability of TraPPE-UA model, we have determined the bulk densities for n-alkanes and compared them to results extracted from the empirical formula of Olabisi and Simha[66,67] as shown in Figure 2. Our results for the n-alkane bulk densities show a very good agreement with the calculations of their empirical equation.

The good behavior of TraPPE-UA pure alkane results enables us to tune the water/n-alkane interaction strengths for only one n-alkane system and then use the resultant parameters for the other n-alkanes. Since the spreading coefficient and contact angles do not depend on the magnitudes of surface tension themselves but on the differences shown in equation (1) and equation (3), we only need to tune the water/n-alkane interaction parameters. The strength of interaction between TIP4P-2005 and TraPPE-UA (ε_{OC}) is tuned for heptane (nC7) at $T = 295\ K$. Heptane (nC7) is chosen because its experimental initial spreading coefficient[1] ($S_{exp} = 0.57$) is fairly close to the transition value, $S = 0$, at $T = 295\ K$. Our tuning parameter r is defined in terms of the Lorentz-Berthelot combining rules as $\varepsilon_{OC} = (1+r)\sqrt{\varepsilon_O \varepsilon_C}$ where ε_O and ε_C are the O-O and nC-nC interactions, respectively.[68,69] The optimal strength of interaction between TIP4P-2005 oxygen atom and TraPPE methyl/methylene groups is found at $r = 0.12$. Therefore, the new interaction strengths of water/n-alkane ε_{OC} for the methyl and methylene groups after this tuning process are $\varepsilon_{OC} = 0.88997$ and $\varepsilon_{OC} = 0.609728$, respectively.

As shown in Figure 3, increasing the interaction strength ε_{OC} by factor $r = 0.12$ effectively enhances the water/n-alkane interfacial tensions at $T = 295K$. Therefore, the new interaction strengths ε_{OC} significantly increased the spreading coefficient of heptane from -7.63 to $0.265\ mN/m$ and decreased the contact angle from

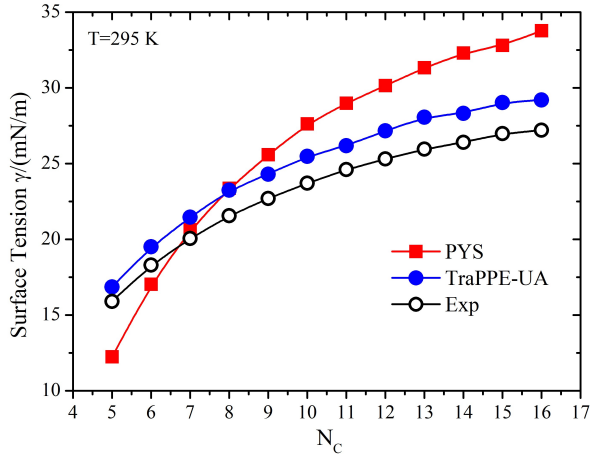

Fig. 1 Chain length (N_c) dependence of surface tension plotted for n-Alkanes: PYS (squares) and TraPPE-UA (filled circles) and compared with surface tension values (open circles) of Goebel and Lunkenheimer.[1] All of the standard errors of the mean are smaller than the marker size, and are not shown here. A table with these values is provided in the electronic supplementary material.

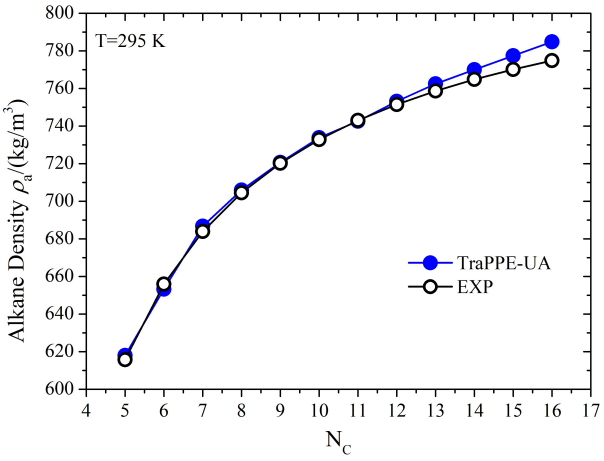

Fig. 2 Chain length (N_c) dependence of bulk densities plotted for n-Alkanes: TraPPE-UA (filled circles) and compared with the values (open circles) extracted from the empirical equation of Olabisi and Simha.[66,67]

about 58° to 0°. This gives us a clear idea about the influential effects of the interaction strengths on thermodynamic properties.[24,25,70,71]

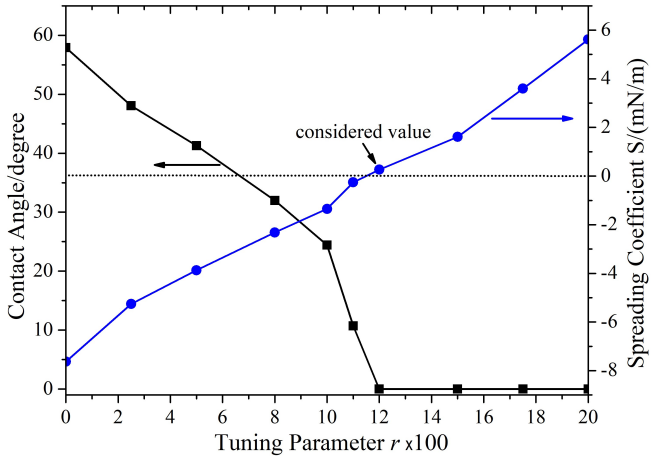

Fig. 3 Spreading coefficient and contact angle are plotted versus the tuning parameter, r. This tuning parameter represents the interaction strength that was defined as ($\varepsilon_{OC} = (1+r)\sqrt{\varepsilon_O \varepsilon_C}$). Dotted line is a guideline to the zero spreading coefficient. Here, simulations are averaged over 50 ns.

Our results of MD simulations of TIP4P-2005/TraPPE-UA interfacial tensions are shown in Figure 4. Fortunately, our results of water/n-alkane interfacial tensions almost have the same gradient as the experimental results. This confirms the validity of using $r = 0.12$ for all the n-alkane chains (nC5-nC16), and not just exclusively for heptane (nC7). The smooth behavior of the Zeppieri et al. values is because they are calculated based on an empirical equation that was derived based on experimental data.[2] Their experimental data were correlated with an equation that depends only on the number of carbon atoms and the temperature to calculate the water/n-alkane interfacial tension. On the other hand, the measurements by Goebel and Lunkenheimer are done under cumulative sequences of purification cycles on their samples which makes their results more reliable.[1]

In addition to the surface tension of pure n-alkanes (Figure 1), we have calculated the surface tension of TIP4P-2005 water at $T = 295K$. The average surface tension of TIP4P-2005 water (averaged over 150 ns) is $\gamma_{wv} = 69.44\ mN/m$ which is relatively close to the experimental value 72.52 mN/m.[72] Then, a set of MD simulations was carried out for water/n-alkane chains (nC5-nC16) with $r = 0.12$ at $T = 295$. Our simulation results are used to calculate the spreading coefficient and contact angle using Eqn. 1 and Eqn. 3, respectively (shown in Figure 5). Simulation results of the water/n-alkane contact angle and spreading coefficient show impressive agreement with those calculated from the experimental data of Goebel and Lunkenheimer[1] and also are close to those calculated from Zeppieri et al.[2] Here, Eqn.1 and Eqn.3 are, respectively, used to calculate the water/n-alkane spreading coefficient and contact angle using the experimental value of water surface tension ($\gamma_{wv} = 72.52$ mN/m) and the experimental values of γ_{wa} and γ_{av}. Thus, there are two independent data sets to confirm the reliability of our MD simulations. These results of the spreading coefficients and contact angles demonstrate that the short n-alkanes (nC5-nC7) spread on the water surface initially, whereas a complete-to-partial initial wetting transition takes place as the n-alkane chain length grows (nC8-nC16). Indeed, this transition was expected at fixed temperature because both the n-alkane/vapor and the water/n-alkane interfacial tensions increase with the chain length N_C. This means that the spreading coefficient, based on the definition in Eqn.1, decreases with increasing N_C. ‡ This transition can be easily observed through the high jump in the contact angle from zero for heptane (nC7) to approximately 25° for octane (nC8) while it then smoothly increases to around 60° for the hexadecane (nC16).

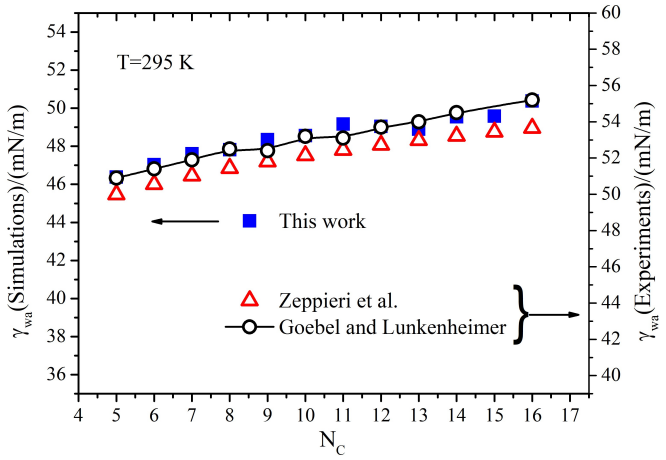

Fig. 4 Chain length (N_c) dependence of interfacial tension plotted for water/n-Alkanes: TIP4P-2005/TraPPE-UA (squares) and compared with Goebel and Lunkenheimer[1] (open circles), and Zeppieri et al.[2] (open triangles) surface tension values. TraPPE-UA results are shifted up by 4.5 mN/m to compare with the experimental data.

Since the water/vapor surface tension is constant at $T = 295K$, the dramatic changes on the water/n-alkane wetting behaviors must be driven by the water/n-alkane and n-alkane/vapor interfacial tensions. To view their effects on the spreading coefficient, we have plotted the second term of Eqn. 1 (we call it $\gamma_{sum} = \gamma_{wa} + \gamma_{av}$) in a vertical plot (ladder plot) which makes the changes in its values more visible (see Figure 6). Although the small n-alkane chains (nC5-nC7) completely wet water surfaces, they have the largest variations in γ_{sum}. This observation indicates that the influence of increasing N_C is larger on the shorter n-alkanes (nC5-nC7) than on the longer ones (nC8-nC16). This could be because the short n-alkanes have a weaker tendency to orient parallel to the interface, than do the longer chains, as we will discuss later. However, the value of γ_{sum} itself must exceed the water/vapor surface tension to have a transition to partial wetting. On other hand, the change in γ_{sum} between nC5 and nC16 ($\Delta\gamma_{sum} \approx 16.3\ mN/m$) is dominated by the change in the n-alkane/vapor surface tension $\Delta\gamma_{av} \approx 12.345\ mN/m$ while the change in the water/n-alkane interfacial tensions is only $\Delta\gamma_{wa} \approx 3.994\ mN/m$ (For comparison, wa-

‡ Ragil et al. previously identified a temperature-dependent wetting transition of pentane on water. They experimentally observed the wetting transition temperature for pentane to be 53 °C.[73]

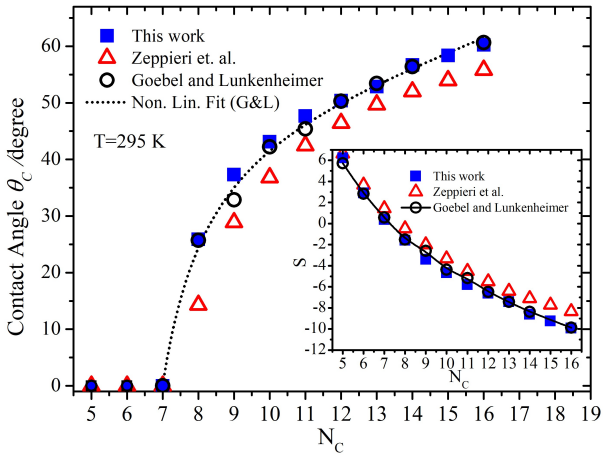

Fig. 5 Chain length (N_c) dependence of contact angle plotted for water/n-Alkanes: TIP4P-2005/TraPPE-UA (squares) and compared with values based on data from Goebel and Lunkenheimer (open circles) and Zeppieri et al. (open triangles). Inset: The corresponding spreading coefficient is plotted vs the n-alkane chain length: TIP4P-2005/TraPPE-UA (squares) and compared with Goebel and Lunkenheimer (open circles), and Zeppieri et al. (open triangles).[1,2] Error bars are smaller than the symbols, and are not shown here. A table with these values is provided in the electronic supplementary material.

ter must be cooled from 295 to 210 K in order to, approximately, get 16 mN/m of change in the water/vapor surface tension). The spreading coefficient of heptane (nC7) is so close to the transition value ($S = 0\ mN/m$), so we can infer that the contact angle increases ≈ 29 degrees for a one carbon atom increase in chain length to octane (nC8) whereas it increases less than two degrees by moving from nC15 to nC16.

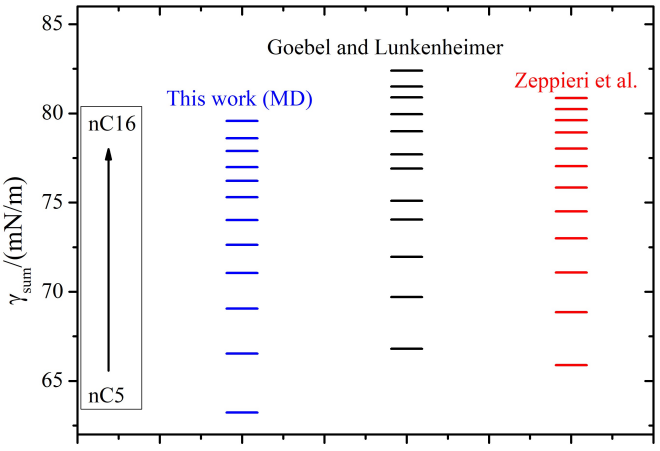

Fig. 6 Ladder plot of ($\gamma_{sum} = \gamma_{wa} + \gamma_{av}$): TIP4P-2005/TraPPE-UA (left) and compared with values based on data from Goebel and Lunkenheimer (middle) and Zeppieri et al. (right).[1,2]

Since the magnitudes of γ_{sum} do not equally change with N_C (as shown in Figure 6), this behavior invites us to investigate the effect of the water/n-alkane interface on the water and n-alkane molecules. The orientation of water molecules and hydrogen bond (HB) number in the water/n-alkane interface are qualitatively described by the charge density profile as shown in Figure 7, where the Gibbs dividing surfaces (GDS) are located at $\rho_W(z) = \rho_A(z)$ and (whenever shown) shifted to $Z = 10\ nm$. Using GROMACS package, the charge density profile is calculated by splitting the simulation box along the longitudinal axis into slices and thereby calculating the average charge in each slice. Charge density profiles in the water/(nC5-nC7) and water/(nC8-nC16) interfaces are different. For water/(nC5-nC7), the charge densities are relatively small and thus we have a lower degree of water orientation and a smaller HB number. For the second group, water/(nC8-nC16), the sharper peaks of charge densities indicate that the orientation of water molecules and the HB number are significantly boosted. This orientation creates two layers of charges in the interfaces (outer one is positive and inner one is negative). Because the number of neighboring water molecules available for HB is small in interfaces, the water molecules orient preferentially to maximize the hydrogen bond number.[3]

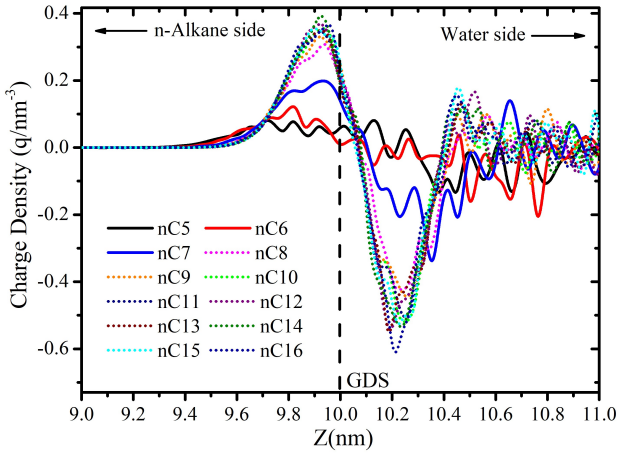

Fig. 7 Charge density profile of water plotted against the location in the interface, Z, normal to the water/n-alkane interface.

The n-alkane chain length also has a significant effect on the interfacial water number density as shown in Figure 8. The water number density profiles also show a discontinuous change between the two groups, water/(nC5-nC7) and water/(nC8-nC16). The apophyses (the local maxima[24,25,74,75]) are smaller and the interfaces are thicker for the shorter alkanes (nC5-nC7) while there is an abrupt increase in the water density (larger apophysis) accompanied by a decrease in the interface thickness for the second group, (nC8-nC16). The results shown in the Figures 7 and 8 indicate that the effects of increasing the n-alkane chain sizes on water is similar to the effect of cooling the system.

Further investigations were performed to assess the effects of water/n-alkane interfaces on the n-alkane density. Apparently, as shown in Figure 9, these effects are long-ranged, manifesting as interfacial layering structures that extend deep into the (nC8-nC16) bulk liquid n-alkane. We also see the dramatic complete-to-partial initial wetting transition in terms of the interfacial thicknesses t as shown in the inset of Figure 9. The interfacial thickness t, represents the interfacial region in the density profile where the density changes from 10% ($z_{10\%}$) to 90% ($z_{90\%}$) of the average bulk liquid density ρ_l. The interfaces are thicker for (nC5-nC7) and thinner for (nC8-nC16). These observations

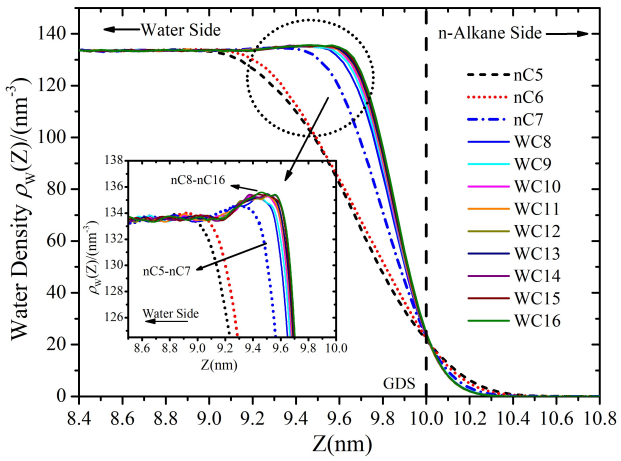

Fig. 8 Number density profile of water plotted against the location in the interface, Z, normal to the water/n-alkane interface. Inset: water density profiles near the water/n-alkane interface.

confirm that the behavior of the water/n-alkane interfaces with increasing n-alkane chain lengths is similar to cooling, i.e., lower temperatures result in thinner interfaces. It is worth mentioning here that the interfaces thicknesses are inversely proportional to the interfacial tensions in agreement with the theoretical prediction, $t^2 \sim \gamma^{-1}$.[23,76,77]

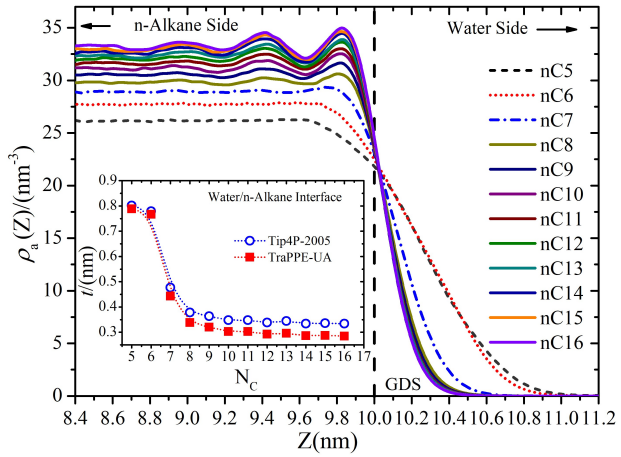

Fig. 9 Density profiles of n-alkane in the water/n-alkane interface plotted against the location in the interface, Z, normal to the water/n-alkane interface. Inset: Interface thickness of water, as shown in Figure 8, (open circles) and n-alkane (squares) versus n-alkane chain length N_C.

We also calculated the n-alkane molecular orientation in terms of the order parameter S_z in the water/n-alkane interface. As shown in Figure 10, the layered n-alkane interfaces (for nC8-nC16) are indicated by the meandering behavior of the order parameter S_z to the left of the Gibbs dividing surface (GDS). An interesting observation is that the minimum S_z values of the short n-alkanes (nC5-nC7) are on the water side of the water/n-alkane interface (to the right of GDS) while those of longer n-alkanes (nC8-nC16) are on the n-alkane side of the interfaces (to the left of GDS). In terms of molecular orientation, this observation is consistent with the results of the water and n-alkane interfacial thicknesses (inset of Figure 9) where the shorter n-alkanes have a weaker tendency to orient parallel to the interface; hence, they have a greater mutual interfacial penetration with water (Figure 11a) while the longer n-alkanes have less mutual penetration (Figure 11b). The order parameter at the GDS is shown in the inset of Figure 10 where a rapid decline occurs at the complete-to-partial initial wetting transition. This behavior is consistent with our results of contact angle and spreading coefficient demonstrating that the complete-to-partial initial wetting transition of water/n-alkane systems occurs with increasing the n-alkane chain lengths.

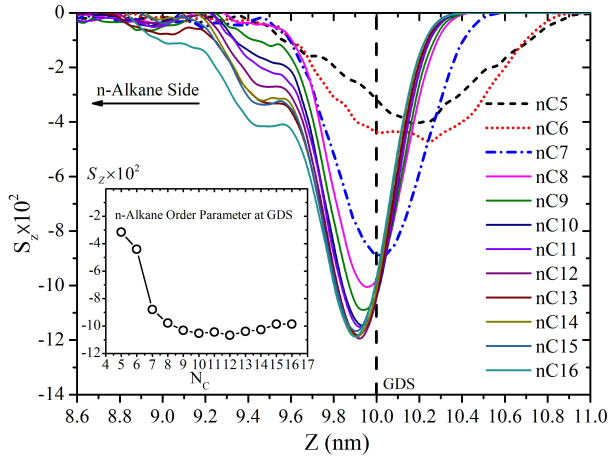

Fig. 10 Orientational order parameter (S_z) of n-alkane molecules in the water/n-alkane interfaces plotted against the location in the interface, Z, normal to the water/n-alkane interface. Inset: Orientation order parameter at Gibbs dividing surface (all shifted to $Z = 10\ nm$) versus n-alkane chain length N_C.

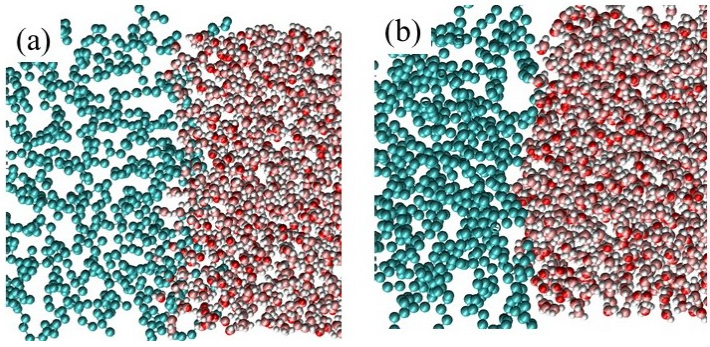

Fig. 11 Snapshots of water/n-alkane interfaces (side view). (a) water/nC5 and (b) water/nC16.

In addition to the moderate increase in alkane ordering for the larger alkanes at the interface, we noted several effects on the molecular conformation of n-alkanes at the interface using the orientational order parameter per atom (explained in the caption of Fig.12). As shown in Figure 12, n-alkane molecules form a nearly "horseshoe" or "C-shaped" structure symmetric about the central segments. Curving of the n-alkane molecules increases as their lengths increase, and they also become more parallel to the interface. Central segments of the n-alkane molecules are more

parallel to the interface than the end segments. This can be understood as the "horseshoe" structure of n-alkane molecules is not exactly parallel to the interface but is slightly rotated about the central segments so the end segments are either closer to water or farther away.

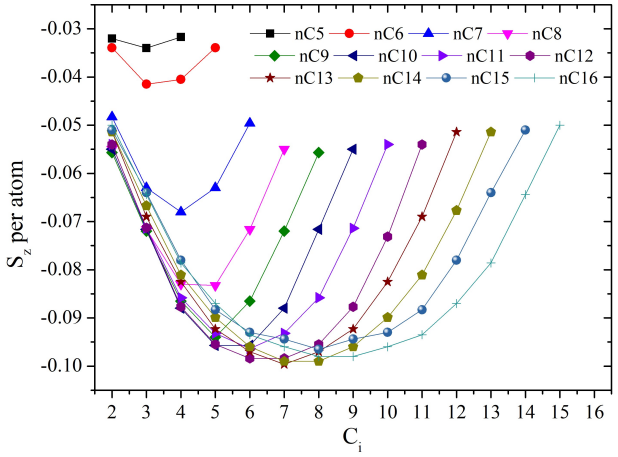

Fig. 12 Orientational order parameter (S_z) per atom of n-alkane molecules in the water/n-alkane interfaces at the Gibbs dividing surface (GDS) plotted against the atom index C_i (For atom i, atoms $i-1$ and $i+1$ are used to calculate $S_z(C_i)$).[78]

To make our results of molecular conformation more visible, as shown in Figure 13, we have calculated the atomic density profiles of undecane, as an example. The undecane atoms are labeled as C3A-C3I and C2A-C2I, respectively, for the methyl and methylene groups, where the central segment is indexed as C2E. We only show half of the density profiles because they are symmetric about C2E. The peaks show that the density of the central segment (C2E) is the highest while the density of the end segment (C3A) is the lowest. This confirms that the edges of the "horseshoe" or "C-shaped" structure in the outer layer are closer to the water.

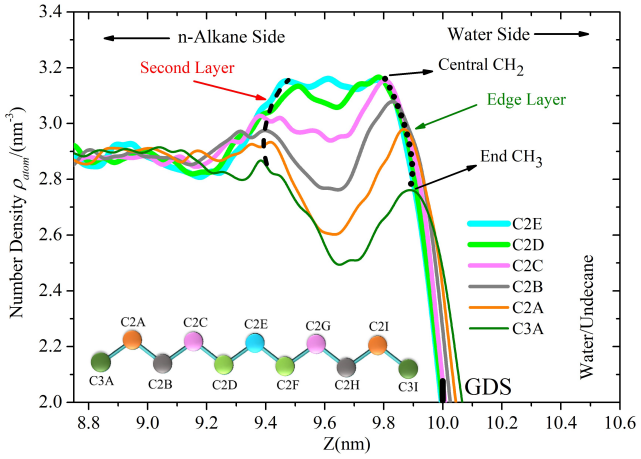

Fig. 13 Number density profiles of undecane (nC11) atoms are plotted against the location in the interface, Z, normal to the water/n-alkane interface. Thick dotted and dashed lines show half of the molecular conformation of undecane (side view) in the outer layer (right) and the second layer (left), respectively.

Using the 3D visual molecular dynamics (VMD) software,[79] Figure 14 shows, as example, a snapshot of the n-alkane molecules in the water/nC16 interface. We see that a majority of the molecules have a "horseshoe" or "C-shaped" structure. Hence, we can consider this observation as a visual confirmation for the "horseshoe" or "C-shaped" geometry to be the average structure of n-alkane molecules in the water/n-alkane interfaces, particularly for nC8-nC16.

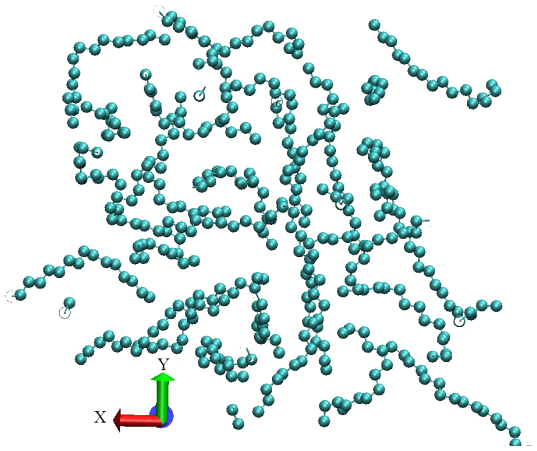

Fig. 14 Snapshot of n-alkane molecules in the water/nC16 interface.

4 Conclusions

We have studied the surface tension of n-alkane systems (nC5 to nC16) using molecular dynamics simulations. We have used two united atoms models in this study, the PYS and TraPPE-UA force fields. The PYS results do not correspond well with the carbon-number behavior of the n-alkane surface tension found by Goebel and Lunkenheimer[1] while the TraPPE-UA results do. Thus, we concentrate on the TraPPE-UA force field in this work. The corresponding water/n-alkane interfacial tensions are calculated at $T = 295\ K$ and used in calculating the spreading coefficient and contact angles of these n-alkanes on water. Water is modeled with the TIP4P-2005 force field and its simulation value of surface tension is 69.437 at $T = 295\ K$. A parameter $r = 0.12$ is used to tune the water/n-alkane interaction strength $\varepsilon_{OC} = (1+r)\sqrt{\varepsilon_O \varepsilon_C}$ to reproduce the wetting behavior of water/Heptane (nC7) at $T = 295\ K$. Our results for the spreading coefficients and contact angles of water/n-alkane systems (with $r = 0.12$) agree very well with experimental results (calculated using the results of Goebel and Lunkenheimer, and Zeppieri et al.).[1,2] They also agree with older estimates of the initial spreading coefficients indicating that the smaller alkanes should all initially wet water perfectly.[80] For short n-alkane molecules, the sum of the interfacial tension of water/n-alkane and n-alkane/vapor (represented by γ_{sum}) is small and thus the complete wetting regime is energetically favorable. It is worth mentioning here that this sum of interfacial tensions is dominated by the n-alkane/vapor interfacial tension. With increasing n-alkane chain length N_C, our results, in agreement with experimental values of surface tension, show faster increase in the n-alkane/vapor tension than in the water/n-alkane interfacial tension. Heptane (nC7) is the longest n-alkane that, at least

initially, completely wets water at $T = 295\ K$. Starting from octane (nC8-nC16), γ_{sum} becomes larger than that of water/vapor, γ_{WV}. This prevents the complete wetting mode from minimizing the surface free energy. Thus, in order to decrease the total surface free energy, n-alkane starts partially dewetting the water surface. This creates three-interface systems (water/n-alkane, water/vapor, and n-alkane/vapor). This partial dewetting reaches an equilibrium state when the three tensions satisfy the relations of Neumann's triangle in which the contact angle increases with increasing γ_{sum} (or increases with N_c).[23]

Further, we have investigated the effects of complete-to-partial initial wetting transitions on several interfacial properties. We have found that the thicknesses of the n-alkane/water interfaces make a strong decrease near this transition but barely vary for the larger n-alkanes. The water density increases in the water/n-alkane interface with increasing n-alkane size, and it is accompanied by molecular re-orientation of water leading to an increase in the number of hydrogen bonds.[3] We investigated this re-orientation by calculating the average charge density along the normal-to-interface director. At the complete-to-partial initial wetting transition, the n-alkane liquid phases near the water/n-alkane interfaces are transformed from relatively homogeneous bulk phases (nC5-nC7) to layered structures (nC8-nC16). The orientation of n-alkane molecules is explored using an orientational order parameter S_z. The n-alkanes are laterally oriented in the water/n-alkane interface which ensures that most of the length of the n-alkane is in close contact with the water.[3,81] Our results show that the larger the n-alkane molecules are, the more parallel to the interface they are.

The conformation of n-alkane molecules is quantitatively investigated by calculating the order parameter per each atom $C_i = 2\cdots(N_C - 1)$. Our results show that the central segments are more laterally oriented than the end ones. This indicates that the n-alkane molecules are not linear but that they systematically curve into "horseshoe" or "C-shaped" structures. To observe how the end segments of the n-alkane molecules orient with respect to the water surface, we have calculated the density profiles of individual n-alkane atoms. We have found that the densities of the central atoms are maximized and that the density decreases systematically for atoms farther from the chain center. We have also observed that the end segments are slightly closer to the water in the outer layer of n-alkane.

In summary, we can say that the main implication of our work is that the wetting state (complete or partial) seems to be reflected in the differences found in the water/n-alkane interfacial structure.

Conflicts of interest

There are no conflicts to declare.

Acknowledgements

We gratefully acknowledge the assistance of Prof. Thomas Vojta in using the Pegasus IV computer cluster in the Physics Department at Missouri S&T. Computational work was also performed using the Foundry HPC supported by the National Science Foundation under Grant No. OAC-1919789.

Notes and references

1 A. Goebel and K. Lunkenheimer, *Langmuir*, 1997, **13**, 369–372.
2 S. Zeppieri, J. Rodríguez and A. L. López de Ramos, *J. Chem. Eng. Data*, 2001, **46**, 1086–1088.
3 H. Xiao, Z. Zhen, H. Sun, X. Cao, Z. Li, X. Song, X. Cui and X. Liu, *Sci. China Chem.*, 2010, **53**, 945–949.
4 D. M. Mitrinović, A. M. Tikhonov, M. Li, Z. Huang and M. L. Schlossman, *Phys. Rev. Lett.*, 2000, **85**, 582.
5 T. R. Underwood and H. C. Greenwell, *Sci. Rep.*, 2018, **8**, 352.
6 F. G. Moore and G. L. Richmond, *Acc. Chem. Res.*, 2008, **41**, 739–748.
7 M. Natália D.S.Cordeiro, *Mol. Simul.*, 2003, **29**, 817–827.
8 R. E. Johnson and R. H. Dettre, *J. Colloid Interface Sci.*, 1966, **21**, 610–622.
9 F. Hauxwell and R. H. Ottewill, *J. Colloid Interface Sci.*, 1970, **34**, 473–479.
10 P. Richmond, B. W. Ninham and R. H. Ottewill, *J. Colloid Interface Sci.*, 1973, **45**, 69–80.
11 C. Del Cerro and G. J. Jameson, *J. Colloid Interface Sci.*, 1980, **78**, 362–375.
12 T. Takii and Y. H. Mori, *J. Colloid Interface Sci.*, 1993, **161**, 31–37.
13 S.-Y. Akatsuka, H. Yoshigiwa and Y. H. Mori, *J. Colloid Interface Sci.*, 1995, **172**, 335–340.
14 K. Ragil, D. Bonn, D. Broseta and J. Meunier, *J. Chem. Phys.*, 1996, **105**, 5160–5167.
15 D. Thanh-Khac Pham and G. J. Hirasaki, *J. Pet. Sci. Eng.*, 1998, **20**, 239–246.
16 T. Pfohl and H. Riegler, *Phys. Rev. Lett.*, 1999, **82**, 783–786.
17 E. Bertrand, D. Bonn, J. Meunier and D. Segal, *Phys. Rev. Lett.*, 2001, **86**, 3208–3208.
18 O.-S. Kwon, H. Jing, K. Shin, X. Wang and S. K. Satija, *Langmuir*, 2007, **23**, 12249–12253.
19 N. Shahidzadeh, D. Bonn, K. Ragil, D. Broseta and J. Meunier, *Phys. Rev. Lett.*, 1998, **80**, 3992–3995.
20 E. Bertrand, H. Dobbs, D. Broseta, J. Indekeu, D. Bonn and J. Meunier, *Phys. Rev. Lett.*, 2000, **85**, 1282–1285.
21 V. C. Weiss and B. Widom, *Phys. A: Stat. Mech. Appl.*, 2001, **292**, 137–145.
22 V. C. Weiss, *J. Chem. Phys.*, 2006, **125**, 084718.
23 J. S. Rowlinson and B. Widom, *Molecular Theory of Capillarity*, Dover Publications, 2002.
24 P. Neupane and G. Wilemski, *Phys. Chem. Chem. Phys.*, 2021, **23**, 14465–14476.
25 Y. Qiu and V. Molinero, *Crystals*, 2017, **7**, 86.
26 R. Mohammadi, J. Wassink and A. Amirfazli, *Langmuir*, 2004, **20**, 9657–9662.
27 Y. Wu, P. J. Shuler, M. Blanco, Y. Tang and W. A. Goddard, SPE/DOE Symposium on Improved Oil Recovery, 2006.
28 T. Schneider and E. Stoll, *Phys. Rev. B*, 1978, **17**, 1302–1322.

29 K. Lunkenheimer and K. D. Wantke, *J. Colloid Interface Sci.*, 1978, **66**, 579–581.

30 P.-L. Chau and A. J. Hardwick, *Mol. Phys.*, 1998, **93**, 511–518.

31 J. G. Harris, *J. Phys. Chem.*, 1992, **96**, 5077–5086.

32 N. Waheed, M. J. Ko and G. C. Rutledge, *Polymer*, 2005, **46**, 8689–8702.

33 N. Waheed, M. S. Lavine and G. C. Rutledge, *J. Chem. Phys.*, 2002, **116**, 2301–2309.

34 W. Paul, D. Y. Yoon and G. D. Smith, *J. Chem. Phys.*, 1995, **103**, 1702–1709.

35 M. G. Martin and J. I. Siepmann, *J. Phys. Chem. B*, 1998, **102**, 2569–2577.

36 S. J. Keasler, S. M. Charan, C. D. Wick, I. G. Economou and J. I. Siepmann, *J. Phys. Chem. B*, 2012, **116**, 11234–11246.

37 K. A. Maerzke, N. E. Schultz, R. B. Ross and J. I. Siepmann, *J. Phys. Chem. B*, 2009, **113**, 6415–6425.

38 L. Zhang and J. I. Siepmann, *J. Phys. Chem. B*, 2005, **109**, 2911–2919.

39 V. P. Modak, H. Pathak, M. Thayer, S. J. Singer and B. E. Wyslouzil, *Phys. Chem. Chem. Phys.*, 2013, **15**, 6783–6795.

40 A. J. Bourque, C. R. Locker and G. C. Rutledge, *J. Phys. Chem. B*, 2017, **121**, 904–911.

41 A. Bourque, C. R. Locker and G. C. Rutledge, *Macromolecules*, 2016, **49**, 3619–3629.

42 P. Yi and G. C. Rutledge, *J. Chem. Phys.*, 2009, **131**, 134902.

43 P. Yi and G. C. Rutledge, *J. Chem. Phys.*, 2011, **135**, 024903.

44 F. Hrahsheh and G. Wilemski, *AIP Conference Proceedings*, 2013, **1527**, 63–66.

45 T. Yamamoto, *Polymer*, 2016, **99**, 721–733.

46 A. Obeidat, F. Hrahsheh and G. Wilemski, *J. Phys. Chem. B*, 2015, **119**, 9304–9311.

47 F. Hrahsheh, Y. S. Wudil and G. Wilemski, *Phys. Chem. Chem. Phys.*, 2017, **19**, 26839–26845.

48 J. L. F. Abascal and C. Vega, *J. Chem. Phys.*, 2005, **123**, 234505.

49 C. Vega and E. de Miguel, *J. Chem. Phys.*, 2007, **126**, 154707.

50 J. Alejandre and G. A. Chapela, *J. Chem. Phys.*, 2010, **132**, 014701.

51 J. M. Míguez, D. González-Salgado, J. L. Legido and M. M. Piñeiro, *J. Chem. Phys.*, 2010, **132**, 184102.

52 R. Sakamaki, A. K. Sum, T. Narumi and K. Yasuoka, *J. Chem. Phys.*, 2011, **134**, 124708.

53 D. Van Der Spoel, E. Lindahl, B. Hess, G. Groenhof, A. E. Mark and H. J. C. Berendsen, *J. Comput. Chem.*, 2005, **26**, 1701–1718.

54 B. Hess, C. Kutzner, D. van der Spoel and E. Lindahl, *J. Chem. Theory Comput.*, 2008, **4**, 435–447.

55 S. Páll, A. Zhmurov, P. Bauer, M. Abraham, M. Lundborg, A. Gray, B. Hess and E. Lindahl, *J. Chem. Phys.*, 2020, **153**, 134110.

56 M. J. Abraham, T. Murtola, R. Schulz, S. Páll, J. C. Smith, B. Hess and E. Lindahl, *SoftwareX*, 2015, **1**, 19–25.

57 W. C. Swope, H. C. Andersen, P. H. Berens and K. R. Wilson, *J. Chem. Phys.*, 1982, **76**, 637–649.

58 G. Bussi, D. Donadio and M. Parrinello, *J. Chem. Phys.*, 2007, **126**, 014101.

59 B. Hess, H. Bekker, H. J. C. Berendsen and J. G. E. M. Fraaije, *J. Comput. Chem.*, 1997, **18**, 1463–1472.

60 T. Darden, D. York and L. Pedersen, *J. Chem. Phys.*, 1993, **98**, 10089–10092.

61 N. M. Fischer, P. J. van Maaren, J. C. Ditz, A. Yildirim and D. van der Spoel, *J. Chem. Theory Comput.*, 2015, **11**, 2938–2944.

62 U. Essmann, L. Perera, M. L. Berkowitz, T. Darden, H. Lee and L. G. Pedersen, *J. Chem. Phys.*, 1995, **103**, 8577–8593.

63 C. L. Wennberg, T. Murtola, B. Hess and E. Lindahl, *J. Chem. Theory Comput.*, 2013, **9**, 3527–3537.

64 P. J. in 't Veld, A. E. Ismail and G. S. Grest, *J. Chem. Phys.*, 2007, **127**, 144711.

65 R. Toutouni, J. Kubelka and M. Piri, *J. Phys. Chem. B*, 2021, **125**, 6658–6669.

66 O. Olabisi and R. Simha, *J. Appl. Polym. Sci.*, 1977, **21**, 149–163.

67 S. K. Nath, J. D. McCoy and J. G. Curro, *Macromolecules*, 1995, **28**, 3275–3281.

68 H. A. Lorentz, *Ann. Phys.*, 1881, **248**, 127–136.

69 D. Berthelot, *Comptes. Rendus. Acad. Sci.*, 1898, **126**, 1703–1855.

70 F. Hrahsheh, *Fluid Ph. Equilibria.*, 2019, **501**, 112272.

71 T. Morawietz, A. Singraber, C. Dellago and J. Behler, *Proc. Natl. Acad. Sci.*, 2016, **113**, 8368–8373.

72 N. B. Vargaftik, B. N. Volkov and L. D. Voljak, *J. Phys. Chem. Ref. Data.*, 1983, **12**, 817–820.

73 K. Ragil, D. Bonn, D. Broseta, J. Indekeu, F. Kalaydjian and J. Meunier, *J. Pet. Sci. Eng.*, 1998, **20**, 177–183.

74 V. P. Modak, B. E. Wyslouzil and S. J. Singer, *J. Chem. Phys.*, 2020, **153**, 224501.

75 X. Wang, K. Binder, C. Chen, T. Koop, U. Pöschl, H. Su and Y. Cheng, *Phys. Chem. Chem. Phys.*, 2019, **21**, 3360–3369.

76 S. Senapati and M. L. Berkowitz, *Phys. Rev. Lett.*, 2001, **87**, 176101.

77 A. Das and S. M. Ali, *J. Mol. Liq.*, 2019, **277**, 217–232.

78 J. Fu and S. G. Urquhart, *Langmuir*, 2007, **23**, 2615–2622.

79 W. Humphrey, A. Dalke and K. Schulten, *J. Mol. Graph.*, 1996, **14**, 33–38.

80 H. Dobbs and D. Bonn, *Langmuir*, 2001, **17**, 4674–4676.

81 G. Rucker, X. Yu and L. Zhang, *Fuel*, 2020, **267**, 117252.